AIAA AVIATION Forum
5-9 June 2017, Denver, Colorado
35th AIAA Applied Aerodynamics Conference

10.2514/6.2017-4216

Subscale Testing of Horizontal-Axis Wind Turbines

Gavin K. Ananda,* Suraj Bansal,† and Michael S. Selig‡
Department of Aerospace Engineering, University of Illinois at Urbana–Champaign, Urbana, IL 61801, USA

This paper discusses the development of wind tunnel test capabilities at the University of Illinois at Urbana-Champaign to obtain the aerodynamic performance of highly-coned subscale wind turbine rotor configurations as part of the ARPA-E funded project to design extreme-scale Segmented Ultralight Morphing Rotors (SUMR). The scaled rotors were designed to be configurable for various coning and pitch angles. Many challenges were associated with testing at these small scales numbers due to the small forces generated, Reynolds number effects, and the high rotor rotation rates required. Rotors were tested at freestream velocities from 4.5 m/s to 9.5 m/s at various coning angles (0 to 50 deg) and pitch angles (4–8 deg). The results obtained can be used to further validate blade element momentum theory (BEMT) codes developed for design and analysis of highly-coned rotors.

I. Introduction

The trend toward the use of large offshore wind turbines in a bid to maximize power production capabilities and reduce overall cost has necessitated the need to build wind turbines with blades longer than 100 m. At these scales, the primary design limitation are structures and weight. Longer blades are required to increase power production; however, the combination of blade bending and gravitational loads mean that to be structurally sound and handle all wind conditions, blade root diameters will reach sizes that are extreme.

The ARPA-E (Advanced Research Projects Agency – Energy) funded SUMR (Segmented Ultralight Morphing Rotor) project intends to address this critical issue and eventually engender the design of 50 MW wind turbines with potentially 200 m long blades. The approach taken is to design downwind wind turbines with blades that are segmented and with the ability to cone. In this way, similar to the swaying and bending of palm trees under high wind loads, the blades can be passively and/or actively coned in such a way that the combination of gravitional, centrifugal, and bending loads acting on the blade are aligned along the blade axis. The alignment of these loads along the axis of the blade, in essence, allows for the blades to be designed to be drastically thinner and lighter.[1,2]

The use of coning for wind turbines is not a novel concept as wind turbine blades are usually preconed to avoid tower strikes. However, coning the wind turbine blades at high angles and the possible use of segmented multiconing is something that has not been explored before. Therefore, a new BEMT code, BladeMorph,[3] is being developed as a part of the ARPA-E SUMR program for the purpose of rapid design and analysis of highly-coned rotors. To validate BladeMorph along with other computational analysis codes for wind turbines, such as AeroDyn[4,5] and PROPID[6,7] and to address the dearth in wind tunnel testing data for high coning angles in literature, a wind tunnel rig was designed and manufactured for subscale testing of horizontal axis wind turbines. Due to many practical limitations, a perfect scaling of the extreme-scale SUMR wind turbine rotors for testing in the UIUC wind tunnel was not achievable. However, since the aim of these experiments was to validate the codes at high coning angles,[3] an entirely new rotor was designed

*Graduate Student (Ph.D. Candidate), 104 S. Wright St., AIAA Student Member. anandak1@illinois.edu
†Graduate Research Assistant, 104 S. Wright St., AIAA Student Member. sbansal5@illinois.edu
‡Professor, 104 S. Wright St., AIAA Associate Fellow. m-selig@illinois.edu

to be tested at low Reynolds number for various coning and pitch angles. Both the freestream velocity and turbine rotation speed (RPM) were also varied, and the measured outputs were power (C_P) and thrust (C_T) coefficients.

This paper is arranged as follows. First, details of the wind turbine rig design and methodology are presented. The blade and hub design and methodology is then presented followed by a method of accurately capturing the coning angle of the rotor when in rotation. Finally, results of wind tunnel tests together with associated discussions are provided.

II. Experimental Apparatus

A. Facility

All experiments were conducted at the low-turbulence subsonic wind tunnel located at the Aerodynamics Research Laboratory at the University of Illinois at Urbana-Champaign (UIUC). The wind tunnel is an open-return tunnel with a rectangular test section that measures 2.8×4.0 ft (0.853×1.219 m) in cross-section and 8 ft (2.438 m) in length. Over the length of the test section, the width of the tunnel cross section increases by approximately 0.5 in (12.7 mm) to account for boundary layer growth along the tunnel side walls. Test section speeds of up to 160 mph (71.53 m/s) can be obtained via a 125 hp (93.25 kW) alternating current electric motor connected to a five-bladed fan. As detailed in Ref. 8, the turbulence intensity of the wind tunnel was measured to be less than 0.1%.

B. Experimental Apparatus

The objective of the wind tunnel tests was to have the ability to measure power (C_P) and thrust (C_T) coefficients as a function of tip speed ratio (TSR) for various coning (β) and pitch (θ) angles.

First, a detailed literature survey was performed on various wind turbine rigs designed to measure C_P and C_T for scaled wind turbines.[9–13] The general conclusions from the literature survey was that the unconed blade diameter should be maximized to ensure that the blade section Reynolds number is maximized. The blade section Reynolds number is maximized to limit low Reynolds number effects. One key limitation to the diameter of the blade is the rotor swept area versus the tunnel cross section area (swept area ratio) which from literature has been between 8–29%. The swept area ratio in this study is maintained to a slightly conservative 20%, resulting in a rotor diameter of 1.5 ft (0.457 m). The range of wind speeds to be tested were 4.5 to 9.5 m/s with the maximum tip speed set to 85 m/s to ensure that blades that were 3D printed did not lose structural integrity when rotating at high speeds. With the tip speed limitation and the range of freestream speeds, the maximum rotation rate was set to 3,500 RPM.

As per the design requirements, the wind turbine rig used for the experiments was custom-designed and in-house fabricated. As shown in Fig. 1, the main force balance is a pendulum-type balance that sits on the ceiling of the wind tunnel. A sting attaches from the force balance to the main turbine rig setup that is located in the center of the tunnel. Since the turbine is oriented downstream, a fairing was designed and 3D printed to minimize the unsteady wake effects from the sting and wind turbine rig and ensure that the flow reaching the turbine blades are smooth. A more detailed side view of the turbine rig is shown in Fig. 2.

The turbine rig consists of a servo motor, inline torque transducer, and turbine blades all attached together via bellows couplings and bearings. The motor is a 200 W Applied Motion servomotor that includes an inbuilt encoder. The motor is rated for 0.55 Nm of continuous torque at a rotation rate of 4,650 RPM. The servomotor is powered by a DC power supply. A regenerative clamp is placed between the DC power supply and the servomotor. It serves as a protection to the power supply when the wind turbine rotor is producing power during testing. An Interface Inc. 1 Nm inline torque tranducer is connected to the servomotor via a bellows coupling. The inline torque tranducer can handle a maximum rotation rate of 8,000 RPM and has no slip rings to ensure minimal torque measurement error. The turbine rotor is connected to the inline torque transducer via another bellows coupling and a bearing block. The bearing block ensures that the shaft of the blade adapter is accurately aligned with the motor and torque transducer shafts thereby minimizing misalignment moments. The adapter used for the turbine rotor hub and blades is a commercial-off-the-shelf R/C propeller adapter. Photographs of the wind turbine rig in the wind tunnel with and without the fairing are shown in Figs. 3(b) and 3(b) respectively.

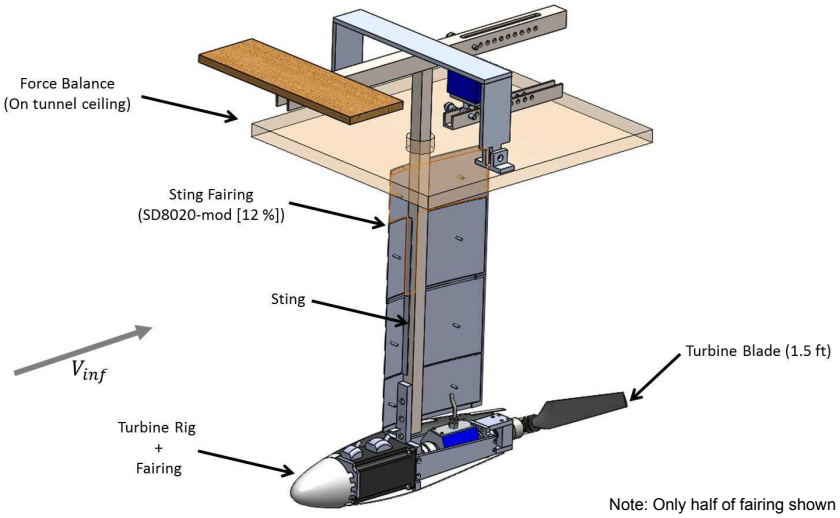

Figure 1. Annotated isometric view of turbine rig setup.

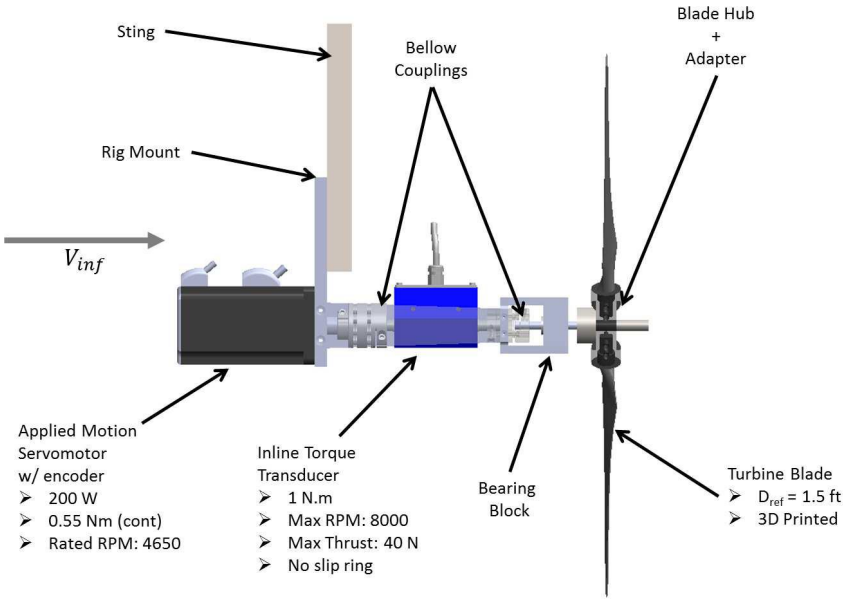

Figure 2. Annotated side view of turbine rig setup.

C. Blade Design

The design goal of the blade was to enable it to operate at low Reynolds numbers with high efficiency while maintaining its stiffness. In this way, nonlinear effects associated with low Reynolds numbers and aeroelastic effects could be minimized to allow for proper validation against computational analysis codes.

The design of the blade itself can be divided into the design of the blade geometry and its individual airfoil sections. Two in-house developed inverse design tools were used for blade design, PROPID[6,7] and PROFOIL.[14,15] PROPID is an inverse design tool used to design the wind turbine blade geometry itself. Based on a specific power requirement and constraints such as maintaining the axial induction factor to

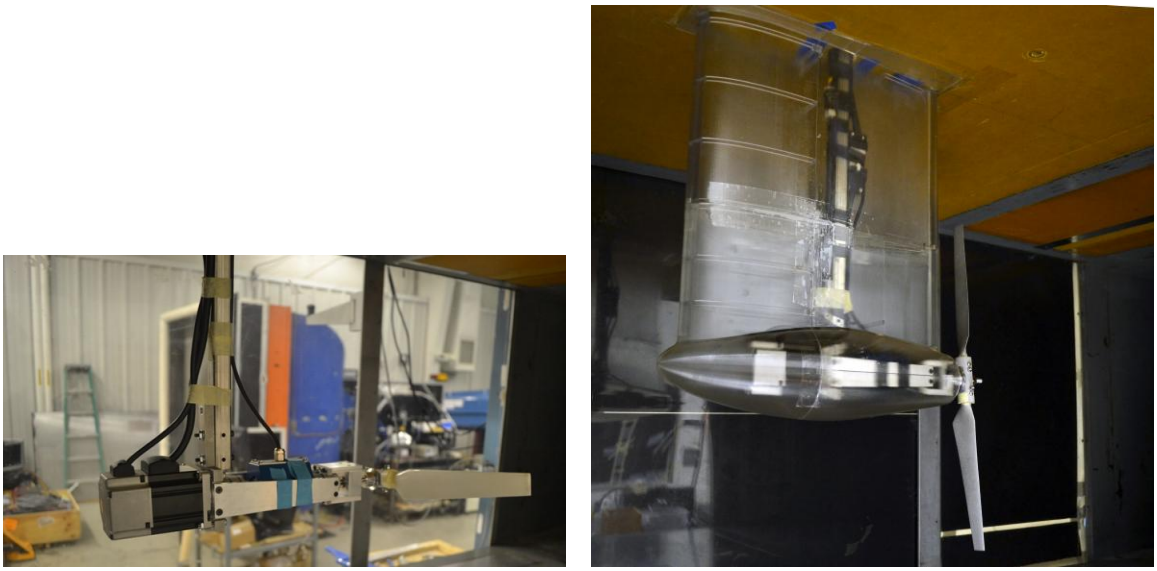

(a) (b)

Figure 3. Photograph of turbine rig: (a) without fairing and (b) with fairing

the Betz optimum (1/3) along the blade, a blade with a prerequisite chord, twist and pitch is inversely designed. The assigned airfoils are designed using PROFOIL, another inverse design tool specifically used for airfoil design. In PROFOIL, the desired velocity distribution, thicknesss, and moment requirements are set a-priori. For the current project, the critical design parameters were that the airfoil was be 10% thick and also have a minimum thickness of 0.75 mm at the trailing edge to ensure 3D printability. Two new airfoils, the AS7004 (root) and AS7005 (tip) were designed in PROFOIL. Both airfoils were based on the SD7003 airfoil.[16] Airfoil coordinates for both airfoils are provided in Appendix A. Table 1 details the chord, twist, and airfoil distribution of the blade tested. The design pitch angle of the blades is 4 deg.

The blades were 3D printed in aluminum from Shapeways[17] and were left un-sanded to minimize blade shape alterations. Aluminum blades were used throughout the tests due to its stiffness, especially for coned tests. For coning angle tests, blades made using materials other than aluminum exhibited large deconing effects when rotating due to its centrifugal loads. Although less, the aluminum blades for coned rotors also exhibited deconing at high rotation rates. These effects are detailed in Section II.C. The planform and sectional view details of the designed blade are shown in Figs. 4(a) and 4(b).

Table 1. Blade Properties

r/R	c/R	Twist	Airfoil
0.05	0.058	6.0	Cylinder
0.15	0.175	23.6	AS7004
0.25	0.165	12.9	Interpolated
0.35	0.155	7.0	Interpolated
0.45	0.145	3.8	Interpolated
0.55	0.135	1.9	Interpolated
0.65	0.125	0.8	Interpolated
0.75	0.115	0.0	Interpolated
0.85	0.105	−0.6	Interpolated
0.95	0.095	−1.9	AS7005

(a) (b)

Figure 4. Blade design details: (a) planform view and (b) airfoil sectional sweep along blade.

D. Hub Design

Rotor hubs were designed to allow for variation of coning angles (β) from 0 to 50 deg and pitch angles (θ) from 4 to 8 deg [see Figs. 5(a,b)]. Since the hub requires less material compared to the blades, multiple hubs of varying cone angle and/or pitch angles were designed. In this way, only one set of blades were used for all tests performed. The hubs were 3D printed in polished metallic plastic (alumide) from Shapeways and sized to ensure structural integrity at all speeds tested.

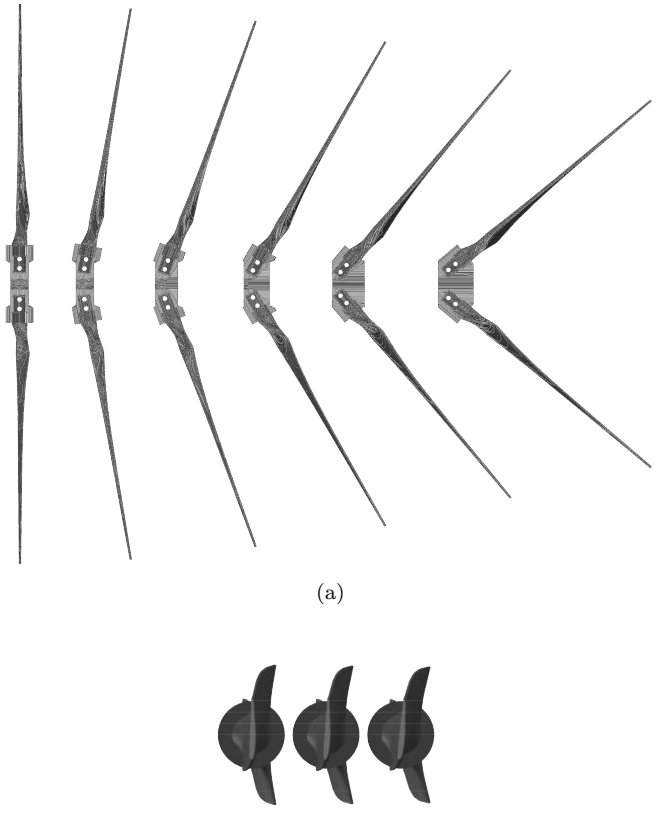

(a)

(b)

Figure 5. CAD model of hub designs: (a) coning angle variation (0, 10, 20, 30, 40, and 50 deg) and (b) pitch angle variation (4, 6, and 8 deg)

III. Methodology

A. Test Matrix

The goal of the wind tunnel tests is to chart the effect of coning angle and pitch angle on rotor performance. A test matrix, shown in Table 2, was created to help accomplish this goal. All tests were conducted at freestream velocities of 15 ft/s (4.6 m/s) to 31 ft/s (9.4 m/s). At each freestream velocity, the rotor speed was varied from a minimum of 500 RPM to a maximum of 3,500 RPM.

Table 2. Test Matrix

Pitch Angle (deg)	Cone Angle (deg)					
4	0	10	20	30	40	50
6	-	-	20	-	40	-
8	-	-	20	-	40	-

B. Measurement Approach

Measurements of the torque are taken with the inline torque transducer. Details of how torque is measured using the rig are shown in Figs. 6(a,b). As shown in Fig. 6(a), with no blade and $V_\infty = 0$, the motor has to overcome the negligible friction of four bearings (in orange and blue) to rotate the shaft. Q_{meas_0} provides the friction torque due to bearings B2, B3, and B4 at each rotation speed. With the blades mounted and $V_\infty > 0$, Q_{meas_1} read by the torque sensor is the aerodynamic torque of the blade less the frictional torque due to bearings, B2, B3, and B4. Finally, the C_P at a specific V_∞ and rotational speed (ω) is calculated by

$$C_P = \frac{(Q_{meas_1} - Q_{meas_0})\omega}{0.5\rho A V_\infty^3} \tag{1}$$

where A is the reference area of the rotor disk based on the unconed radius, R_{ref}.

The thrust coefficient, C_T, of the turbine is calculated from the measurements taken using the load cell located on the ceiling of wind turbine rig (see Fig. 1). Given that the force balance is of a pendulum type, any drag acting on the turbine blades will be measured by this load cell. The fairings for the sting and turbine rig are not attached to the force balance but to the ceiling of the wind tunnel. As a result, only the drag (D_{meas}) of the turbine blades is measured by the load cell. The C_T is then calculated by

$$C_T = \frac{D_{meas}}{0.5\rho A V_\infty^2} \tag{2}$$

It should be noted that both C_P and C_T have been calculated using projected unconed rotor area. The tip speed ratio (TSR) results presented in this paper is calculated by

$$TSR = \frac{\omega R \cos(\beta)}{V} \tag{3}$$

Lastly, all results provided in this paper do not include wind tunnel corrections.

C. Deconing Effects

During testing of coned rotors, deconing of the aluminum blades were observed due to the centrifugal forces associated with the blade rotating at high speeds. As a result, a method of capturing the amount of deconing of the rotor as a function of rotation rate was required to ensure that the rotor performance was accurately understood. Deconing of the rotors was captured using a strobe light. At each rotation rate, a photograph of the side view of the rotor was captured by adjusting the frequency of the strobe light such that the rotating rotor appeared still and oriented vertically (stroboscopic effect).

Strobe light photographs were captured at rotor rotation rates of 0, 500, 900, 1300, 1700, 2100, 2500, and 2900 RPM for all cone angles tested (10, 20, 30, 40, 50 deg). Figures 7–11 shows a sample of these photographs at rotation rates of 0, 500, 1300, 2100, and 2900 RPM. It can be observed that the blades decone nonlinearly meaning that each radial section of the blade operates at a different cone angle. The

effective cone angle of the rotor is calculated by taking the tangent of the blade at the 75% radial location of the blade. The effective cone angles measured directly from the strobe light photographs are tabulated in Table 3. Note that the strobe light photographs presented are at zero V_∞ (wind tunnel off). Strobe light photographs taken at V_∞ of 31 ft/s showed negligible deconing differences to the zero V_∞ cases.

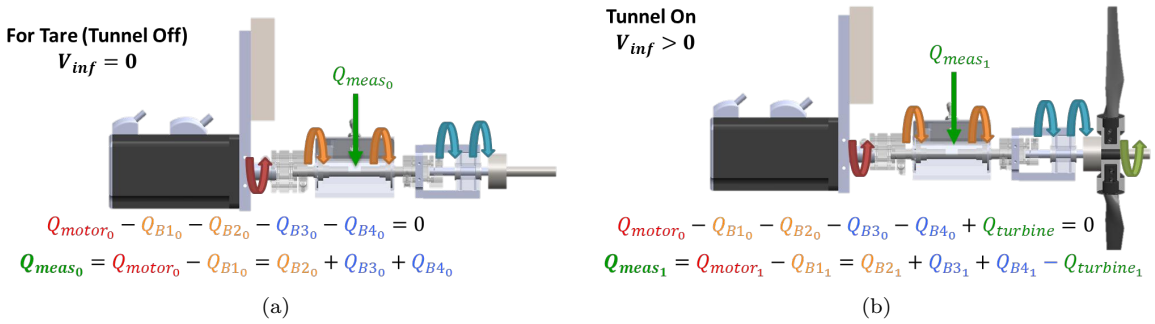

Figure 6. Annotated view of moments affecting the torque calculations: (a) $V_\infty = 0$ and (b) $V_\infty > 0$

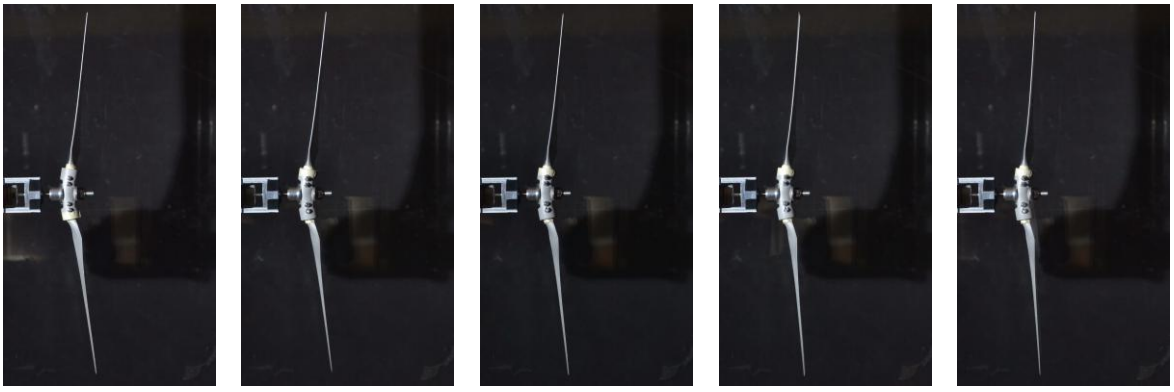

Figure 7. Strobe light photos showing deconing of blades for a rotor with 10 deg coning and with a rotation rate of (a) 0, (b) 500 RPM, (c) 1300 RPM, (d) 2100 RPM, and (e) 2900 RPM.

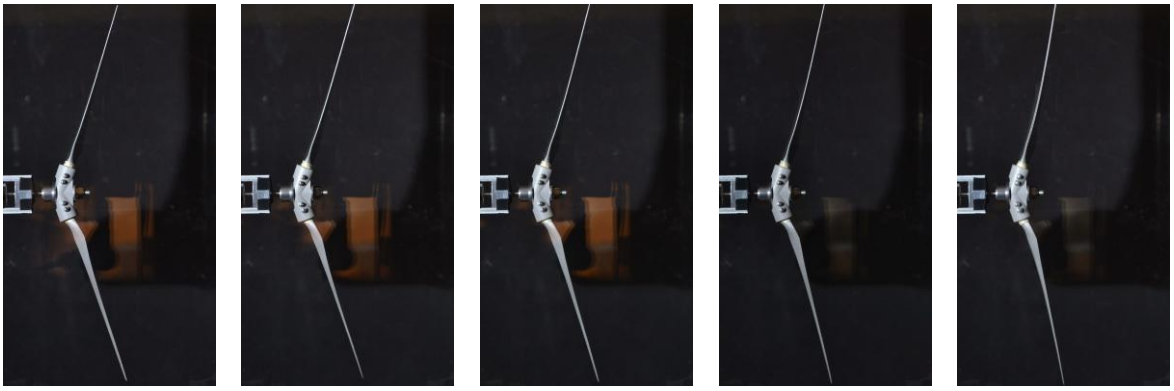

Figure 8. Strobe light photos showing deconing of blades for a rotor with 20 deg coning and with a rotation rate of (a) 0, (b) 500 RPM, (c) 1300 RPM, (d) 2100 RPM, and (e) 2900 RPM.

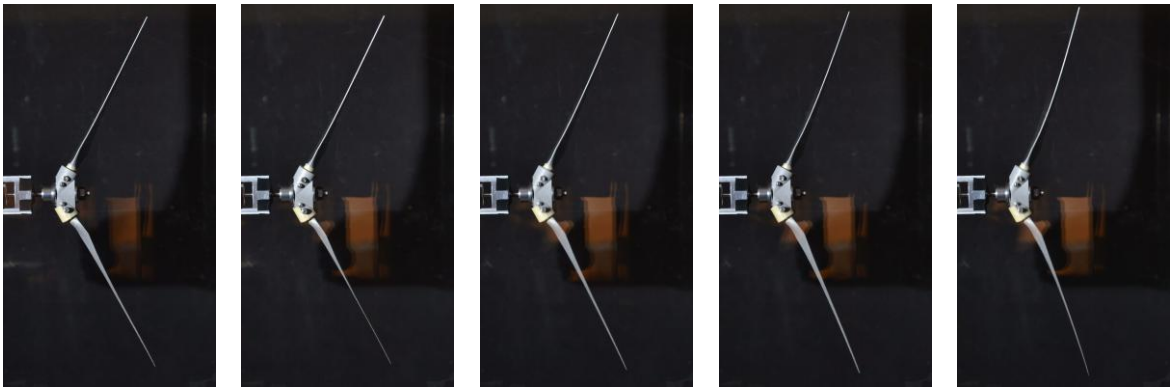

(a) (b) (c) (d) (e)

Figure 9. Strobe light photos showing deconing of blades for a rotor with 30 deg coning and with a rotation rate of (a) 0, (b) 500 RPM, (c) 1300 RPM, (d) 2100 RPM, and (e) 2900 RPM.

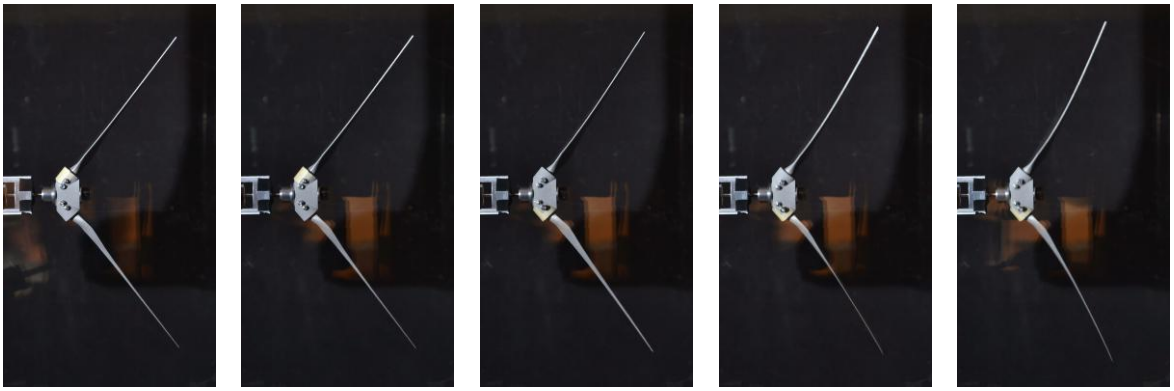

(a) (b) (c) (d) (e)

Figure 10. Strobe light photos showing deconing of blades for a rotor with 40 deg coning and with a rotation rate of (a) 0, (b) 500 RPM, (c) 1300 RPM, (d) 2100 RPM, and (e) 2900 RPM.

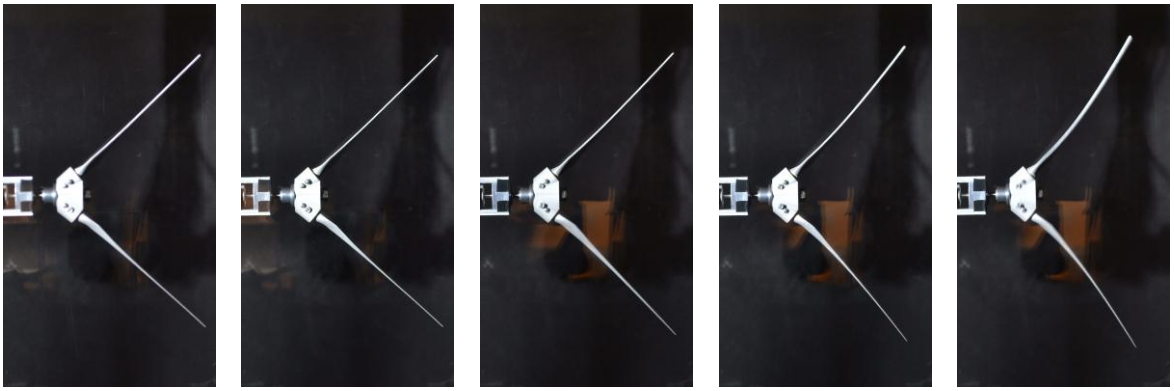

(a) (b) (c) (d) (e)

Figure 11. Strobe light photos showing deconing of blades for a rotor with 50 deg coning and with a rotation rate of (a) 0, (b) 500 RPM, (c) 1300 RPM, (d) 2100 RPM, and (e) 2900 RPM.

Table 3. Rotor Effective Cone Angle as a Function of Rotation Rate as Measured from the 75% Blade Span

Design Cone Angle (deg)	10	20	30	40	50
Rotation Rate (RPM)	Effective Cone Angle (deg)				
0	8.1	18.5	28.1	38.5	47.0
500	7.5	18.0	27.5	37.8	46.5
900	6.3	16.5	26.0	35.8	45.5
1300	5.4	15.5	24.8	34.1	44.8
1700	5.0	14.8	22.9	32.3	42.5
2100	4.2	13.8	21.1	30.5	39.8
2500	3.6	12.8	19.0	27.6	35.7
2900	3.2	10.8	16.9	25.3	33.2

IV. Results and Discussion

Wind tunnel runs were conducted with the aluminum blades tested at various freestream velocities. Test velocities ranged from 15 ft/s (4.6 m/s) to 31 ft/s (9.4 m/s). The range of rotation rates tested for the turbine were from 500 to 3,500 RPM. The range of freestream velocities and rotation rates results in tip speed ratios (TSR) from 1 to 12.

A. Reynolds Number Effects

One of the main issues with testing scaled blades is the effect of Reynolds numbers. At low Reynolds numbers ($Re < 500{,}000$), airfoil viscous effects related to the laminar separation bubble start to play a large role in the performance of the blade itself. As a result, it is important to test rotors at the highest freestream speeds possible. However, higher freestream speeds concurrently require higher rotation rates for the rotor to achieve similar tip speed ratios. Each blade coning and pitch setting was tested at wind tunnel freestream speeds up to 31 ft/s. Figure 12 shows the effect of freestream velocity on C_P of the rotor with a pitch of 4 deg and coning angle of 0 deg.

Figure 12 clearly shows the correct trends of C_P as a function of TSR. As V_∞ increases, the overall curve

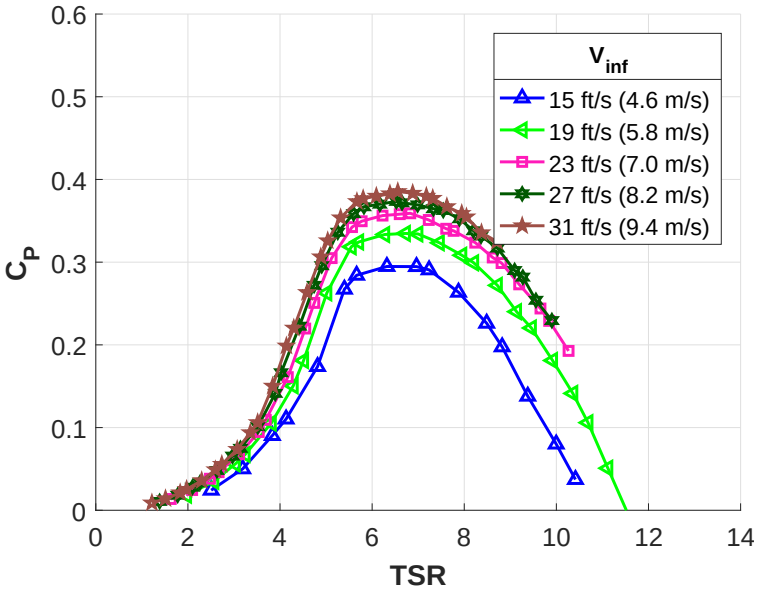

Figure 12. C_P vs TSR curves for rotor at 4 deg pitch and 0 deg coning.

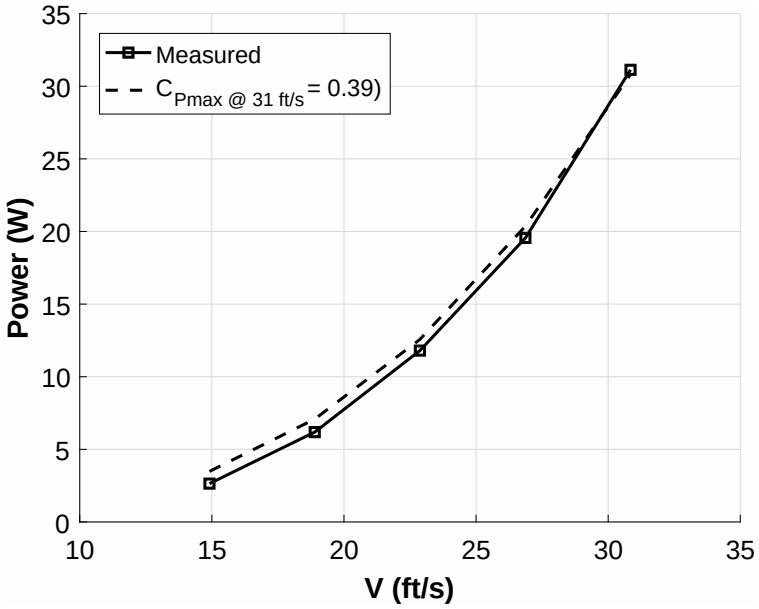

Figure 13. Power vs V_∞ curve for rotor at 4 deg pitch and 0 deg coning.

also shifts up. Similar to what has been observed in the literature, the main reason for the curve shift is the Reynolds number effects associated with the blade. As V_∞ increases, the blade sectional Reynolds number increases. Consequently the efficiency of the airfoil increases, thereby increasing the airfoil C_l and mainly decreasing its C_d. As can be observed from the curves, as V_∞ reaches velocities close to 10 m/s, Reynolds number effects start to minimize as the C_P vs TSR curves start to converge.

An interesting way of looking at the results is in terms of a normal operation of a wind turbine. At a particular wind speed, the rotor is expected to be operating at the tip speed ratio that maximizes C_P. Therefore, the power curve of the rotor is plotted from the data in Fig. 13 (blue line with square markers). The effect of Reynolds number can be seen by coplotting the theoretical power curve (blue dashed line) given a C_{Pmax} at 31 ft/s of 0.39. The rotor is observed to produce lower power at lower wind speeds.

B. Cone Angle Variation

In this section, the effect of varying cone angle on the aerodynamic performance of the rotor was investigated. Different hubs were individually designed for a specific coning angle configuration. Whenever the coning angle of the rotor had to be changed, the hub designed for the corresponding coning angle was selected and operated with the same set of blades each time to obtain the wind tunnel test data. Coning angles of 0, 10, 20, 30, 40, and 50 deg were tested for the design pitch case of 4 deg. The results of these tests at a freestream velocity of 31 ft/s are shown in Fig. 14.

As noted in Section III.C., blades of highly coned rotors operating at high rotational speeds exhibited deconing due to centrifugal loads along the rotor blade length. Hence, it should be noted that each curve in Fig. 14 corresponds to the cone angle at which the rotor was designed to operate instead of the actual coning angle of the rotor during rotation. Figure 15 shows the same results with rotation rate as the x-axis instead of tip speed ratio. As can be seen from Fig. 15, the peak region on C_P vs rotation rate curves for higher coning angles are flatter compared to the zero coning case, with the 10 deg coning case being the outlier. The flattening of the regions near the C_P peaks suggests higher C_P than expected at higher rotational speeds. The higher-than-expected values of C_P can be explained via deconing of blades at higher rotational speeds. The higher the rotational speeds, the larger the decrease in effective coning angle of the rotor (see Table 3). The fact that the outboard region of the rotor blade operates at a lower coning angle at higher rotational speeds suggests higher C_P at higher rotor speeds given that a major portion of the power from the rotor

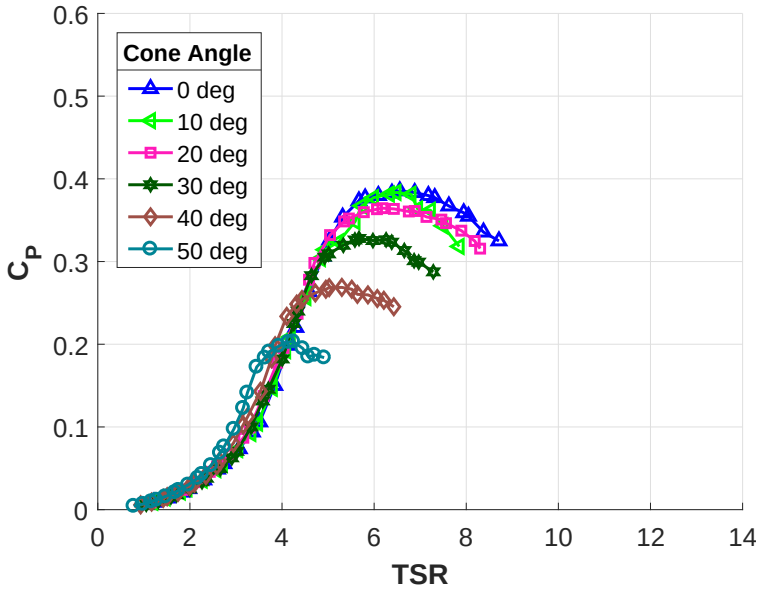

Figure 14. C_P **vs** TSR **curves for rotor at 4 deg pitch and** V_∞ **of 31 ft/s.**

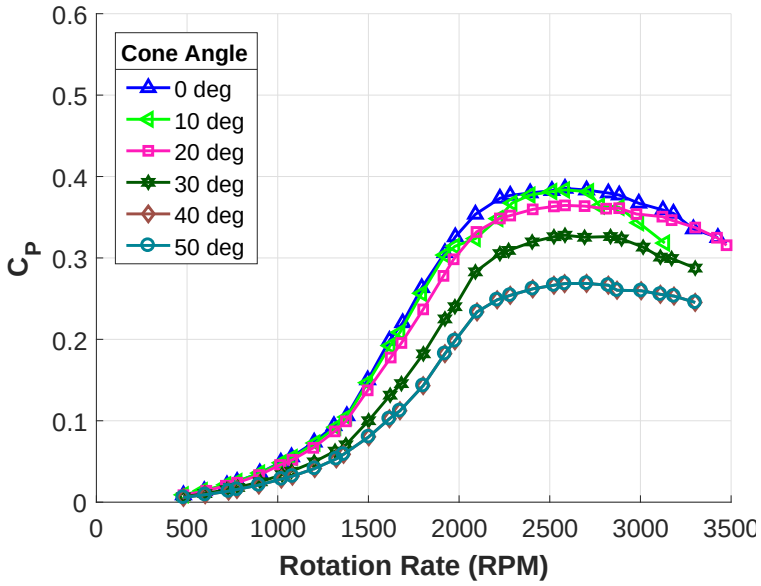

Figure 15. C_P **vs Rotation Rate curves for rotor at 4 deg pitch and** V_∞ **of 31 ft/s.**

is generated from the outboard sections of the blades. For 10 deg coning case, there were high vibrations observed at higher rotational speeds, thus causing a deviation from the trend of C_P peak flattening at higher coning angles due to deconing.

From Figs. 14 and 15, it can be seen that with higher coning, the $C_{P_{max}}$ values occur at lower values of TSR. Such a trend of decreasing values of optimum TSR with higher coning can be attributed to a reduction in the angles of attack experienced by the blades when the coning angle is increased. The reduction in the angles of attack along the blade at higher cone angles stems from a changed flowfield geometry on the blades where only a component of the axial velocity normal to the blades contribute toward generation of

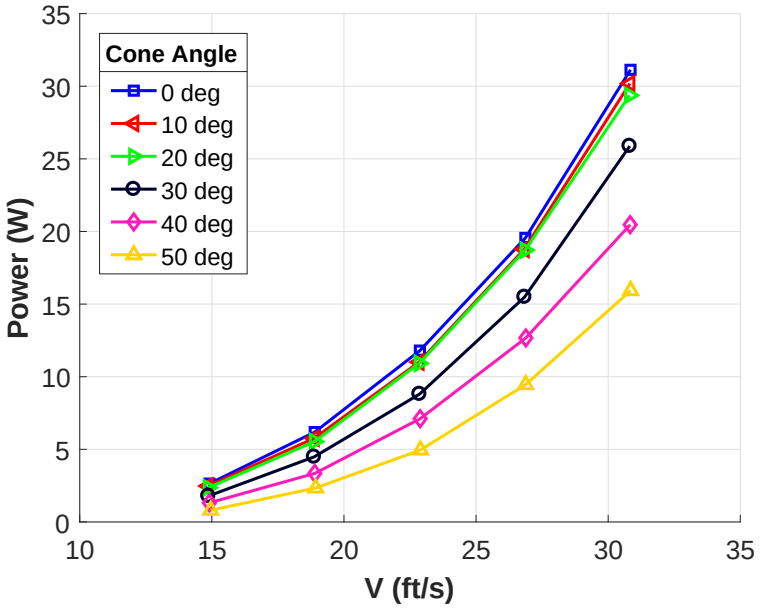

Figure 16. Optimal Power vs V_∞ curves at various coning angles.

aerodynamic forces, for a given tip speed ratio. It should be noted that the blades were designed to operate at a specified L/D distribution at zero cone angle. Keeping the aforementioned fact in mind and the fact that higher TSR values lead to a larger angles of attack along the blade, it becomes apparent for higher coning angle cases, the angles of attack for which the optimum L/D distribution is obtained, are achieved at lower TSR values.

Similar to the prior subsection, power curves for the rotor at the different coning angles are coplotted in Fig. 16. The power curves were created by using the power values that related to $C_{P_{max}}$ of the rotor at the specific freestream velocity tested. Results from Fig. 16 shows the clear reduction in power production with increasing coning angle.

C. Pitch Angle Variation

Figures 17 and 18 show measured C_P vs TSR curves for the wind turbine blades at pitch angles, θ of 2, 4, and 6 deg at coning angles of 20 and 40 deg. From these results, it can be observed that C_P decreases with increasing pitch angle. The reduction in C_P values when the blades are increasingly pitched to feather (increasing pitch angles) is because for the same tip speed ratios, pitching the blades to feather decreases angles of attack along the blades, thereby generating lower torque at the same freestream and rotational speeds. In addition, the TSR at which maximum C_P occurs shifts lower with increasing pitch angle. The decrease in optimum TSR values occur again due to a reduction in angles of attack values along the blade. As explained earlier, a combination of the increase in angles of attack due to operating at lower TSR and the decrease in the same with pitching the blades to feather causes the angles of attack for optimum L/D distribution to occur at a lower TSR value. It is also interesting to see that the effect of changing the pitch of the blades at higher coning on the C_P reduces at higher coning angle, as seen in Figs. 17 and 18.

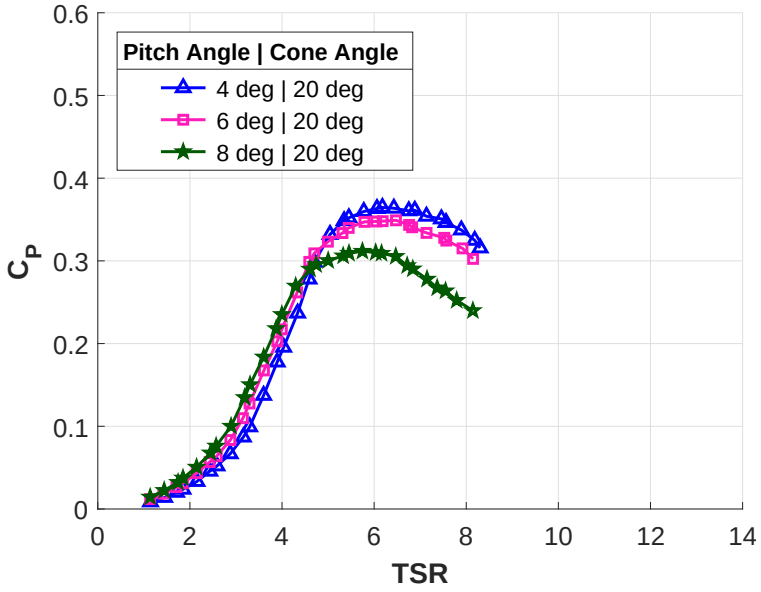

Figure 17. C_P **vs** TSR **for rotor at 20 deg coning and** V_∞ **of 31 ft/s.**

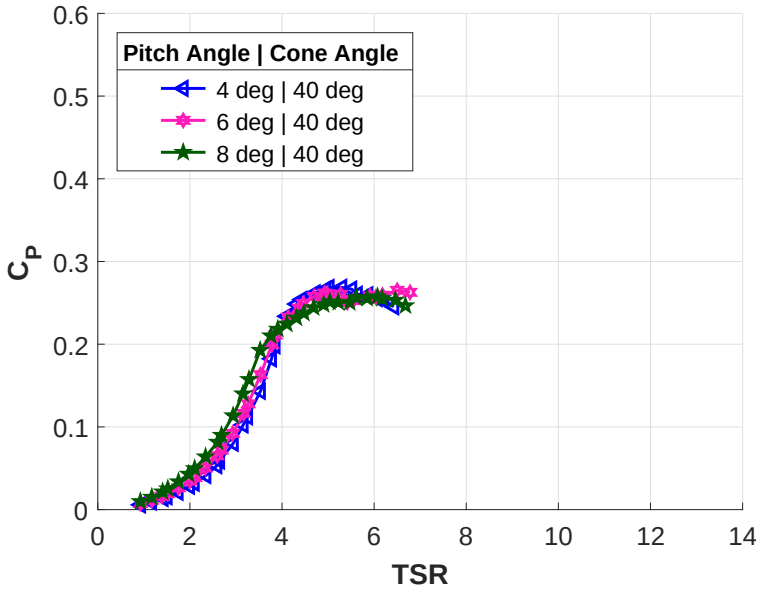

Figure 18. C_P **vs** TSR **for rotor at 40 deg coning and** V_∞ **of 31 ft/s.**

V. Conclusions

The ARPA-E funded SUMR program intends to address and overcome the issues associated with the trends toward extremely large offshore wind turbine designs (up to 50 MW). In order to deal with the structural and weight contraints at these sizes, a passive/active segmented coning concept is proposed. Current computational design and analysis codes for HAWT wind turbines have not been validated at high coning angles. In addition, there is no literature available regarding wind tunnel tests for wind turbines at high coning angles. To address this issue, a wind tunnel rig was designed to measure C_P and C_T as a function of tip speed ratio for wind turbine blades of varying coning and pitch angles. Wind tunnel tests were conducted on rotors with coning angles up to 50 deg and varying pitch angles. The results obtained will be used for validation of BEMT codes developed for analysis of highly coned rotors.[3]

VI. Acknowledgment

The information, data, or work presented herein was funded in part by the Advanced Research Projects Agency-Energy (ARPA-E), U.S. Department of Energy, under Award Number DE-AR0000667. The views and opinions of authors expressed herein do not necessarily state or reflect those of the United States Government or any agency thereof.

References

[1]Loth, E., Ichter, B., Selig, M. S., and Moriarty, P. J., "Downwind Pre-Aligned Rotor for a 13.2 MW Wind Turbine," AIAA Paper 2015-1661, 33rd Wind Energy Symposium, AIAA Scitech, Kissimmee, Florida, January 2015.

[2]Ichter, B., Steele, A., Loth, E., and Moriarty, P. J., "Structural Design and Analysis of a Segmented Ultralight Morphing Rotor (SUMR) for Extreme-Scale Wind Turbines," AIAA Paper 2012-3270, 42nd AIAA Fluid Dynamics Conference and Exhibit, New Orleans, Louisiana, June 2012.

[3]Bansal, S., Ananda, G. K., and Selig, M. S., "Development of an Aerodynamic Analysis Methodology for Segmented Ultralight Morphing Rotors," AIAA Paper 2017-4217, 35th AIAA Applied Aerodynamics Conference, Denver, CO, June 2017.

[4]Moriarty, P. J. and Hansen, A. C., "AeroDyn Theory Manual," NREL/EL 500-36881, Golden, CO, 2005.

[5]Jonkman, J. M., Jonkman, G. J., and Damiani, R. R., "AeroDyn v15 User's Guide and Theory Manual," NREL, Golden, CO, 2015.

[6]Selig, M. S. and Tangler, J. L., "Development and Application of a Multipoint Inverse Design Method for Horizontal Axis Wind Turbines," *Wind Engineering*, Vol. 19, No. 5, 1995, pp. 91–105.

[7]Selig, M. S., "PROPID – Software for Horizontal-Axis Wind Turbine Design and Analysis," `http://www.ae.illinois.edu/m-selig/propid.html`, 1995–.

[8]Selig, M. S., *Summary of Low-Speed Airfoil Data, Vol. 4*, SoarTech Publications, Virginia Beach, Virginia, 2005.

[9]Van Treuren, K. W. and Gregg, J. R., "Testing Rotating Horizontal Axis Wind Turbine Blade Designs in a Laboratory Wind Tunnel," Tech. Rep. GT2010-23575, Proceedings of ASME Turbo Expo 2010: Power for Land, Sea, and Air, Glasgow, UK, June 2010.

[10]Bahaj, A. S., Molland, A. F., Chaplin, J. R., and Batten, W. M. J., "Power and Thrust Measurements of Marine Current Turbines under Various Hydrodynamic Flow Conditions in a Cavitation Tunnel and a Towing Tank," *Renewable Energy*, Vol. 32, March 2007, pp. 407–426.

[11]Monteiro, J. P., Silvestre, M. R., Piggott, H., and Andre, J. C., "Wind Tunnel Testing of a Horizontal Axis Wind Turbine Rotor and Comparison with Simulations from Two Blade Element Codes," *Journal of Wind Engineering and Industrial Aerodynamics*, Vol. 123, October 2013, pp. 99–106.

[12]Krogstad, P. A. and Lund, J. A., "An Experimental and Numerical Study of the Performance of a Model Turbine," *Wind Energy*, Vol. 15, June 2012, pp. 443–457.

[13]Krogstad, P. A. and Adaramola, M. S., "Performance and Near Wake Measurements of a Model Horizontal Axis Wind Turbine," *Wind Energy*, Vol. 15, September 2012, pp. 743–756.

[14]Selig, M. S. and Maughmer, M. D., "Generalized Multipoint Inverse Airfoil Design," *AIAA Journal*, Vol. 30, No. 11, 1992, pp. 2618–2625.

[15]Selig, M. S., *Multi-Point Inverse Design of Isolated Airfoils and Airfoils in Cascade in Incompressible Flow*, Ph.D. thesis, Dept. of Aerospace Engineering, Pennsylvania State Univ., University Park, PA, May 1992.

[16]Selig, M. S., Donovan, J. F., and Fraser, D. B., *Airfoils at Low Speeds*, Soartech 8, SoarTech Publications, Virginia Beach, Virginia, 1989.

[17]Shapeways, "3D Printing," `http://www.shapeways.com`, Accessed June. 2017.

A Tabulated Airfoil Coordinates

AS7004
root

x/c	y/c
0.996647	0.009636
0.986982	0.010830
0.971763	0.013177
0.951540	0.016219
0.926404	0.019551
0.896440	0.023175
0.862032	0.027144
0.823642	0.031413
0.781766	0.035913
0.736940	0.040551
0.689728	0.045222
0.640719	0.049790
0.590478	0.054073
0.539532	0.057933
0.488429	0.061265
0.437723	0.063956
0.387946	0.065887
0.339606	0.066960
0.293175	0.067074
0.249083	0.066167
0.207731	0.064197
0.169481	0.061152
0.134654	0.057023
0.103507	0.051849
0.076258	0.045686
0.053054	0.038647
0.034004	0.030868
0.019120	0.022567
0.008442	0.014145
0.002076	0.005922
0.000108	-0.001335
0.003526	-0.007684
0.012470	-0.013660
0.026255	-0.018937
0.045038	-0.023272
0.068821	-0.026767
0.097384	-0.029526
0.130414	-0.031563
0.167586	-0.032878
0.208548	-0.033508
0.252883	-0.033530
0.300119	-0.033006
0.349729	-0.032032
0.401142	-0.030666
0.453771	-0.028960
0.507021	-0.026967
0.560294	-0.024720
0.612993	-0.022268
0.664593	-0.019602
0.714645	-0.016857
0.762576	-0.014317
0.807708	-0.012128
0.849395	-0.010379
0.887027	-0.009116
0.920034	-0.008343
0.947902	-0.008018
0.970207	-0.008071
0.986569	-0.008443
0.996612	-0.009027
1.000001	-0.009353

AS7005
tip

x/c	y/c
0.996691	0.018505
0.987150	0.019346
0.972121	0.021308
0.952137	0.023910
0.927271	0.026738
0.897588	0.029787
0.863444	0.033111
0.825274	0.036671
0.783550	0.040414
0.738783	0.044271
0.691515	0.048167
0.642320	0.052016
0.591796	0.055721
0.540560	0.059160
0.489198	0.062167
0.438261	0.064610
0.388285	0.066359
0.339778	0.067303
0.293213	0.067333
0.249018	0.066377
0.207592	0.064389
0.169299	0.061345
0.134454	0.057230
0.103313	0.052077
0.076087	0.045933
0.052920	0.038907
0.033915	0.031127
0.019074	0.022807
0.008434	0.014348
0.002089	0.006060
0.000098	-0.001299
0.003436	-0.007739
0.012261	-0.013752
0.025918	-0.019027
0.044583	-0.023322
0.068276	-0.026750
0.096785	-0.029432
0.129802	-0.031393
0.167004	-0.032645
0.208041	-0.033235
0.252498	-0.033249
0.299899	-0.032763
0.349719	-0.031881
0.401381	-0.030671
0.454295	-0.029195
0.507861	-0.027517
0.561478	-0.025682
0.614549	-0.023762
0.666493	-0.021820
0.716749	-0.019962
0.764704	-0.018353
0.809710	-0.017076
0.851156	-0.016177
0.888467	-0.015673
0.921114	-0.015553
0.948625	-0.015768
0.970618	-0.016256
0.986750	-0.016988
0.996655	-0.017903
1.000000	-0.018368